Citation: Using Polarized Total Synchronous Fluorescence Spectroscopy (pTSFS) with PARAFAC analysis for Characterizing Intrinsic Protein Emission. M. Steiner-Browne, S. Elcoroaristizabal, and A.G. Ryder. *Chemometrics and Intelligent Laboratory Systems*, 194, 103871, (**2019**). DOI: 10.1016/j.chemolab.2019.103871

Using Polarized Total Synchronous Fluorescence Spectroscopy (pTSFS) with PARAFAC analysis for Characterizing Intrinsic Protein Emission.

Marina Steiner-Browne, Saioa Elcoroaristizabal, and Alan G. Ryder*

Nanoscale BioPhotonics Laboratory, School of Chemistry, National University of Ireland, Galway, H91CF50, Galway, Ireland.

[Author version, corrected version.]

* Corresponding author.
Prof. Alan G. Ryder,
Nanoscale Biophotonics Laboratory, School of Chemistry,
National University of Ireland – Galway, Galway, H91 CF50, Ireland.

Tel: 353-91-492943; Fax: 353-91-552756; Email: alan.ryder@nuigalway.ie

Abstract

Using polarized Excitation Emission Matrix (pEEM) spectroscopy to measure the intrinsic emission of proteins offers a potentially useful methodology for a wide variety of potential applications. However, the presence of Rayleigh light scatter causes significant problems when attempting to use Parallel Factor (PARAFAC) and for anisotropy calculations. The use of polarized Total Synchronous Fluorescence Spectroscopy (pTSFS) can minimize Rayleigh scatter and avoid the use of complex data correction methods. Here, we investigated for the first time the use of pTSFS and PARAFAC to analyze the intrinsic emission of an Immunoglobulin (IgG) type protein in its native state. To enable PARAFAC analysis however, TSFS data (which is not trilinear) must first be transformed into an EEM like layout (t-EEM) and this generated a region with no experimentally acquired information (<8%). Here we critically evaluated several data handling methods and determined that interpolation was the best solution for dealing with the spectral regions with no experimentally acquired data at the blue edge of the emission.

There were only subtle structural changes measured over temperature range (15−35°C) analyzed and PARAFAC only resolved two emitting components. A Trp emission component (average signal from all Trp present) which represented >92% of the explained variance, and a much weaker, mostly Tyr related emission with ~3% of the explained variance. The recovery of this Tyr component was only possible because TSFS measurements were less contaminated by Rayleigh scattering. Changes in Tyr-to-Trp energy transfer rates caused by thermal motion were detected as an increase in Tyr contribution, which could not be resolved with the equivalent pEEM measurements due to light scatter contamination. The increased selectivity, sensitivity, and reproducibility of pTSFS measurements shows that this is a better

option than pEEM for fluorescence emission based monitoring of protein structural change or lot-to-lot variance of IgG type proteins.

Keywords: Immunoglobulin G, Fluorescence, Multidimensional, Spectroscopy, Anisotropy, PARAFAC.

1 Introduction

The use of intrinsic fluorescence spectroscopy (IFS) to characterize protein structural change in solution [1] is potentially very useful for the characterization of therapeutic proteins such as the Immunoglobulin G (IgG). IgG type proteins have many features which make them attractive therapeutic agents [2, 3], however, efficacy is very dependent on both tertiary and quaternary structure [4]. Phenylalanine (Phe), tyrosine (Tyr), and/or tryptophan (Trp) fluorophores are present in most proteins, which allows the use of IFS to characterize protein structural change in solution [1]. Protein intrinsic fluorescence emission is dominated by Trp when present, with Tyr and Phe contributing much less due to their lower quantum yields and Förster resonance energy transfer (FRET) processes [1, 5]. Furthermore, Trp emission is highly sensitive to environmental changes [6], making it a particularly useful tool for monitoring protein structural changes [7-10]. Tyr emission is insensitive to changes in solvent polarity, but is affected by changes in FRET, which potentially provides information about conformational changes and size [1, 7, 11]. Tyr emits at ~305 nm, which means that the emission is highly affected by Rayleigh light scatter contamination at the blue edge and overlap with Trp fluorescence at the red edge of its emission. This makes resolving the Tyr signal very challenging and spectral deconvolution methods are usually required [12-14]. For IgG which has twice as many Tyr fluorophores (~50/60) as Trp (~20/30) and with many being positioned within the Förster radius of each other, it means that homo- and hetero-FRET is extensive, resulting in Trp dominant emission. In many cases the application of IFS for analytical protein studies use simple 2D spectra or single excitation/emission wavelength pairs, which take no advantage of all the spectral information available in the full excitation and emission space. Therefore, the use of multidimensional fluorescence spectroscopy (MDF) offers a potentially better approach to retrieving more useful information from multi-fluorophore proteins.

The commonest MDF measurement techniques for intrinsic fluorescence are Excitation-Emission Matrix (EEM) [15] and Total Synchronous Fluorescence Spectroscopy (TSFS) [16]. These provide a 3D spectral signature of the multiple fluorophores present in a protein or a complex mixture [17-19]. TSFS is potentially more useful than EEM for blue edge emission analysis because it is less affected by the first order Rayleigh scattering (RS) interference in the raw data and thus require much less or no data pre-processing for scattering removal compared to EEM. Thus, TSFS measurements may preserve more spectral information from the blue edge of protein emission and in particular the Tyr component. Furthermore, the presence of light scatter has a very large and adverse effect on anisotropy measurements which makes its elimination a priority.

Anisotropy resolved multidimensional emission spectroscopy (ARMES) is a combination of anisotropy, MDF measurements, and chemometrics [9]. ARMES uses anisotropy (r) as an additional layer of photophysical information in combination with the intensity (I), excitation wavelength (λ_{ex}), and emission wavelength (λ_{em}). ARMES provides extra information that can help better characterize changes

in intrinsic protein fluorescence by better resolving the emission of individual fluorophores. For multi-fluorophore proteins, anisotropy varies across the fluorescence emission space (*aniso*-MDF map) which is due to the presence of multiple fluorophores and the interactions (*e.g.* FRET) among these fluorophores [19, 20]. Thus, *aniso*-MDF maps are very sensitive to protein structure changes, which make these maps a good diagnostic tool for evaluating protein changes (unfolding, refolding, and aggregation) [9]. Multi-way decomposition methods, such as multivariate curve resolution (MCR) [21, 22] and parallel factor analysis (PARAFAC) [23-25] are required to resolve fluorophore contributions from MDF data [26, 27] which is a critical part of ARMES.

ARMES using TSFS measurements was previously used for the resolution and identification of individual fluorophores in relatively simple proteins with one or two Trp fluorophores [9, 28]. This data, however, was polarizer dependent with no excitation below ~300 nm. The use of wire grid polarizers permitted excitation below 300 nm and thus collection of a more complete excitation-emission space including Tyr excitation/emission [20]. A previous study of ours [29], showed that for IgG, polarized EEM (pEEM) measurements were adversely affected by residual Rayleigh scatter, and it affected PARAFAC resolution of Tyr and Trp at the emission blue edge, λ_{em}<320 nm, particularly for the parallel polarized emission. Solving this issue, requires the use of more costly spectrometers with improved stray light rejection (double emission monochromators) and/or the use of reduced emission slits to increase spectral resolution (but at the cost of signal-to-noise ratio), which is not always practical or feasible with standard benchtop instruments. TSFS therefore becomes the most practical option to overcome scattering issues and to enable better spectral resolution at the emission blue edge. As TSFS lacks trilinearity required for PARAFAC analysis a simple transformation into an EEM like layout (t-EEM) was required [30]. However, this t-EEM transformation generates regions with no experimentally acquired spectral data, that is the absent spectral data region (ASDR), and this could have a negative impact on PARAFAC modelling.

Here we explore the use of TSFS to try to better characterize the fluorescence emission of native state rIgG over a small temperature range compared to the previous PEEM/PARAFAC analysis where the Rayleigh scatter issue was a significant problem [29]. A critical factor was to deal with the ASDR, and here we evaluated the impact of using three different methods: missing data, insertion of zeros [31], and interpolation [32] on the PARAFAC model output (component profiles and scores). Of particular importance is the recovery of Tyr fluorescence from the blue edge of the emission which was badly affected by Rayleigh scatter contamination in PEEM measurements.

2 Materials and methods

2.1 Materials

A 0.01 M Phosphate 0.150 M saline buffer (PBS) at pH 6.5±0.1 was prepared with sodium phosphate monobasic, sodium phosphate dibasic hepta-hydrate and sodium chloride (purchased from Sigma-Aldrich and used without further purification), which were dissolved in HPLC grade high purity water (HPW) purchased from Honeywell. PBS buffer was used to reconstitute IgG from rabbit serum (≥95% essentially salt-free, lyophilized powder) that was purchased from Sigma-Aldrich and used without further purification. Aseptic sample preparation techniques were used to minimize contamination. Three

rabbit IgG (rIgG) solutions were prepared in PBS buffer (1.1 ± 0.2 mg mL^{-1}); from three vials that were acquired at the same time and with the same lot number (SLBM2617V). Polyethersulfone (PES) Captiva Premium Syringe 0.2 µm filters (Agilent) were used to filter the solutions. The three rIgG solutions had a final concentration of 1.3 mg mL^{-1}, 0.9 mg mL^{-1}, and 1.2 mg mL^{-1}, for R1, R2, and R3, respectively. Lobind Eppendorf tubes (1.5 mL) were used to separate aliquots (enough for one measurement) of each rIgG solution and stored at −70°C before use (over 11 weeks). Freshly prepared samples were immediately stored at −70°C, without making any measurements. Prior to making spectroscopic measurements, each aliquot was slowly defrosted overnight at 4−8°C.

2.2 Instrumentation and data collection

UV-visible and fluorescence measurements were made using conditions as previously described [29] and details are provided in the supplemental information. Slit widths (10 nm), scan rate (1200 nm mn^{-1}) and photomultiplier tube (PMT) detector voltage of 650 V were used [29] for all measurements. Polarized TSFS (pTSFS) were collected using an excitation range of λ_{ex}=240−320 nm (same as pEEM), and $\Delta\lambda$ interval of 20−210 nm at 2 nm step increments in each case. pTSFS measurements were extended until the red edge of the Trp emission (λ_{em}>450 nm) at each λ_{ex}, in order to ensure comparability with previous pEEM based studies (Figure 1). TSFS measurements took approximately 10 minutes per polarization setting, and thus 40 minutes in total per temperature. To characterize native state emission, rIgG solutions, in triplicate, were measured at nine different temperatures (15°, 17°, 20°, 23°, 25°, 27°, 30°, 33° and 35°C), and solutions were thermally equilibrated for five minutes at each temperature. Spectra were uncorrected for instrument response, which is also dependent on polarizer transmittance.

2.3 Data analysis and chemometric methods

PLS_Toolbox ver. 8.2.1 (Eigenvector Research Inc.), FluorS (in-house written program) were carried out in MATLAB ver. 9.1.0 (The Mathworks Inc.) for the data analysis. TSFS behaves as a non-bilinear matrix, meaning that the spectral shape and emission intensity of each fluorophore varies as $\Delta\lambda$ changes (*vide infra*). Thus, each fluorophore in TSFS does not have a unique synchronous fluorescence spectrum and this prevents direct PARAFAC analysis, unless data restructuring is performed to generate trilinearity. Three-way TSFS data could be directly decomposed by bilinear methods like MCR-ALS [17, 19, 21, 22, 31, 33, 34], resolving the spectral profile of each fluorophore if proper data augmentation is performed and suitable designed sample sets are used [35, 36]. However, in the case of IgG intrinsic emission, the emission of individual fluorophores have very different intensities, degrees of spectral overlap, and are non-radiatively connected, and in general experimental design cannot be implemented which could break these dependencies [31, 33]. Thus, the trilinearity required for PARAFAC might help when analyzing the highly overlapped emission of IgG. In addition, PARAFAC of this pTSFS data can be directly compared with PARAFAC modelling of similar pEEM data [29], to unambiguously determine which measurement method is superior in the context of protein analysis.

$TSFS_{HV}$ and $TSFS_{HH}$ measurements were used to calculate the G-factor ($G=I_{HV}/I_{HH}$, Figures S1/S3, SI) and this was used to correct the $TSFS_{VH}$ spectra, giving the corrected perpendicular $TSFS_{\perp}$ spectra (Figure S2, SI) [29]. The $TSFS_{VV}$ spectra are the parallel polarized, $TSFS_{\parallel}$, spectra. The total unpolarized $TSFS_T$ spectra were calculated from the pTSFS spectra as follows: $TSFS_T=TSFS_{\parallel}+2\times TSFS_{\perp}$, and were used to compare the outputs of modeling polarized TSFS

measurements compared to the simpler, and more common unpolarized TSFS measurements [1, 29, 37, 38]. The polarized datasets, TSFS$_{\parallel}$ and TSFS$_{\perp}$, were then subjected to Raman scattering minimization and inner filter effect (IFE) correction [38].

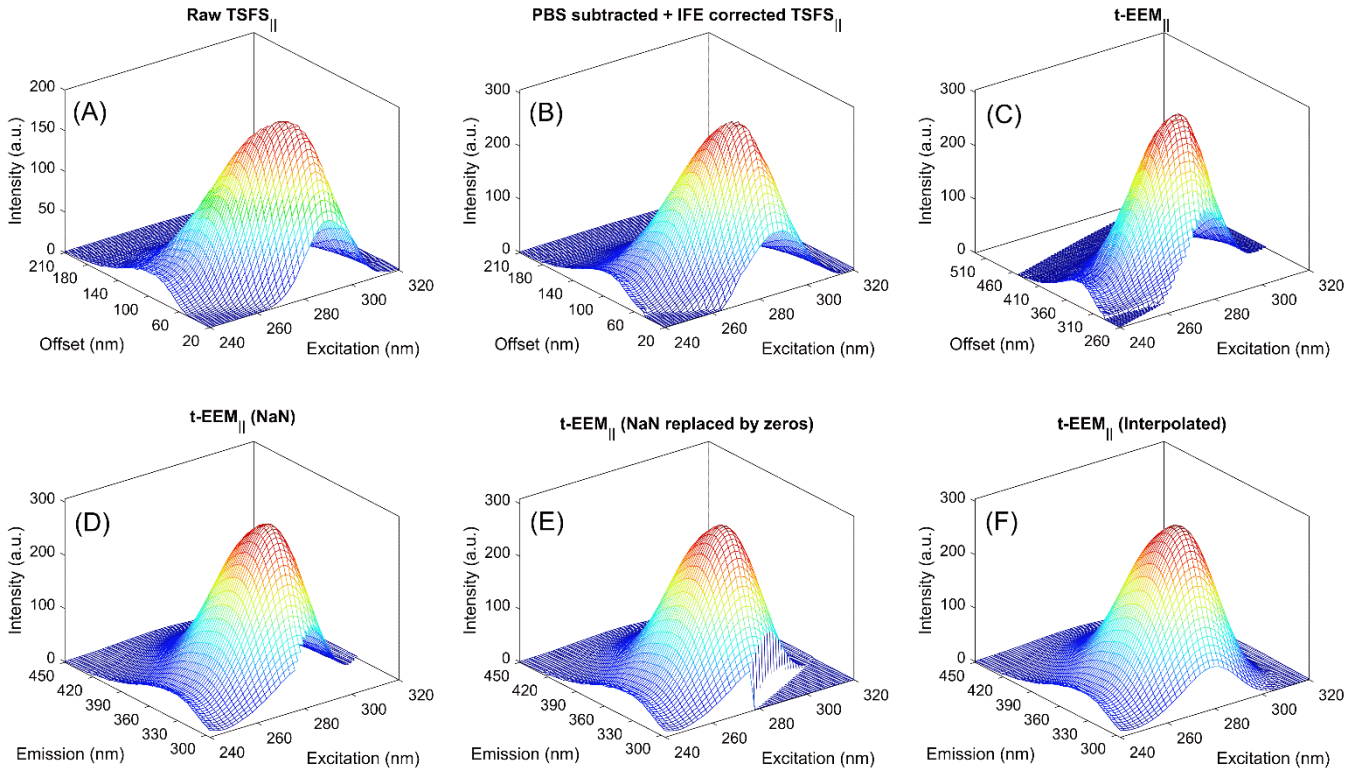

Figure 1: (A) Raw pTSFS$_{\parallel}$ spectra of rIgG native state measured at 20°C. (B) TSFS$_{\parallel}$ PBS subtracted, and IFE corrected. (C) TSFS$_{\parallel}$ data was converted into t-EEM$_{\parallel}$. (D) t-EEM$_{\parallel}$ spectra were cut at λ_{em} 296−450 nm to remove most of the noisy area produced by IFE correction. (E) The areas outside the first Rayleigh scattering were replaced by zeros. (F) The t-EEM$_{\parallel}$ spectra were interpolated and smoothed.

The use of wavelength offsets, $\Delta\lambda \geq 20$ nm, minimizes the collection of Rayleigh scattered light (Figure 1) and thus, Raman bands were the major source of scattered light [1]. However, the relatively wide slit widths (10 nm) coupled with the very short Stokes shifted emission for excitation wavelengths of <300 nm means that some light scatter will be present. If the sample solution contains particles, then this will increase further due to Mie and Tyndall scattering. Raman scattering was easily removed with a blank subtraction (PBS buffer spectrum) from the TSFS spectrum (Figure 1B). IFE correction was necessary due to the high optical density (Abs=0.31±0.05, at 280 nm, 2 mm pathlength) of the protein solutions (Figure S4, SI) [39, 40]. The absorbance-based approach [1] using the limit of reporting (LOR) [39] as a guide was implemented as previously described [29]. The polarized MDF measurements yield much weaker fluorescence intensity than unpolarized MDF measurements [9], making the IFE correction a critical step for accurate PARAFAC resolution and anisotropy calculations.

The TSFS emission spectral range of $\Delta\lambda$=20−210 nm yielded matrices of 27 samples × 96 $\Delta\lambda$ × 41 λ_{ex}, which were then rearranged into t-EEM (Figure 1C), generating matrices of 27 samples × 136 λ_{em} × 41 λ_{ex} [17, 31]. The weak emission bellow $\lambda_{em} \leq 292$ nm was mainly due to noise, which was amplified by

IFE correction (Figure 1C). To both eliminate IFE correction artifacts and to make the pTSFS data equivalent to the pEEM data, the t-EEM data was reduced to λ_{em}=296−450 nm, generating matrices of 27 samples × 78 λ_{em} × 41 λ_{ex} (Figure 1D). The removed short emission wavelength was mostly related to weak Tyr emission as well as the blue edge of Trp emission [1, 28]. The weak Tyr emission in the t-EEM datasets was less affected than the same Tyr emission in the pEEM datasets [29], because of the much reduced scattered light contamination.

The t-EEM data (Figure 1C) as collected had a large number of co-ordinates (λ_{ex}, λ_{em}) with no intensity data (~30%) [31], the absent spectral data region (ASDR). This was reduced (Figure 1D) to a much smaller region (~8%) when the spectra were edited down to the λ_{em}=296−450 nm range used for data analysis. The use of missing data to deal with the ASDR makes PARAFAC free to estimate a continuous profile for the spectral components. Unfortunately, these solutions can easily be distorted, leading to discontinuities and sharp peaks, [41] due to the presence of IFE correction induced artifacts, residual light scatter and noise, in the short wavelength emission regions which are close to these missing values. These factors are exacerbated here by the poor polarizer transmittance and instrument performance in the 250–300 nm region. The other solutions for facilitating PARAFAC modelling were either to replace the ASDR with zeros (Figure 1E) [42] or use interpolated values (Figure 1F). However, while using zeros may facilitate PARAFAC convergence [42], here the ASDR, contains the short Stokes shifted emission (both Tyr and Trp) region. This means that imposing a zero value, artificially distorts the true emission data being used for modelling, and this can lead to incorrect spectral profiles being recovered from the PARAFAC models [32]. The use of interpolation has been previously proven to obtain chemically meaningful solution on EEM data [32], however, it has never been used to reconstruct t-EEM data or that from protein emission. As with the other methods, areas with low SNR and residual scatter close to the ASDR will adversely affect PARAFAC. One issue with interpolation of protein emission is validating that the reconstructed emission is the true emission and that artifacts are not introduced. The use of interpolation for addressing the ASDR issue has been explored [17, 30, 31] but with a very different sample system.

Once the IFE and ASDR corrections had been implemented, the standard anisotropy [1] formula (Equation S1, SI) was used to calculate the anisotropy (r) at each emission wavelength, and then used to build *aniso*-MDF maps (λ_{ex} × λ_{em} × r) [38]. Finally, for PARAFAC analysis, the t-EEM data were then normalized (by peak maximum), to remove variances introduced by small concentration differences and in day-to-day measurements, to more clearly show the real spectral changes being induced by structural change [23].

For PARAFAC analysis, the number of components was selected based on several criteria: the CORe CONsistency DIAgnostic test (CONCORDIA) [23], on how much of variance was explained by the model (Table S1, SI), and visual inspection of the recovered spectral profiles and residuals. Validation of spectral deconvolution results were performed using split-half analysis. PARAFAC analysis was applied with non-negative constraints for all modes (sample, λ_{em}, λ_{ex}) using the best-fitting model as initialization method (from various test models fitted with a small number of iterations) [25, 32]. First, the t-EEM datasets containing missing data, filled with zeros and interpolated were analyzed by PARAFAC to see if the different emitters could be resolved and if there were differences in the recovered loadings (spectra) for the different emission polarization states. Once sensible models and components had been generated,

anisotropy spectra for the recovered components were calculated. PARAFAC resolution of t-EEM were then compared with that previously obtained from the same samples measured with pEEM [29].

3 Results and discussion

3.1 2D spectral analysis of MDF methods

Two-dimensional spectra were used first to evaluate the spectral information obtained in the t-EEM and pEEM measurements, considering the differences between Trp and Tyr emission, Tyr-to-Trp FRET, and the amount of spectral variations produced over a 15−35°C temperature range [29]. The difference in the recovered Tyr emission peak maxima (Figure 2, gray spectra): t-EEM$_T$ (312 nm) and EEM$_T$ (316 nm) was caused by the EEM Rayleigh scatter correction procedure. This removed part of the weak Tyr signal which overlapped the Rayleigh scatter, leaving only the Tyr emission that overlapped with Trp emission. The shape of the 2D t-EEM data was very similar to that extracted from pEEM measurements except that the Tyr emission was stronger in the t-EEM data (Figure 2). The difference spectra showed that Tyr fluorescence [12] corresponded to <5% of the EEM$_T$ (Figure 2C/D) but ~13% of the t-EEM$_T$ (Figure 2A/B) spectra. The better quality of the t-EEM data is also revealed by the smaller anisotropy values obtained at short emission wavelengths (λ_{em}<320 nm). The recovered anisotropy values (Figure 2B) now agree better with what one might expect from a system where there is extensive FRET from Tyr to Trp, and where at least some of the Trp residues are directly excited with relatively high anisotropies [1]. These we expect to be the Trp residues located in the hydrophobic environments and thus at the blue side of the peak.

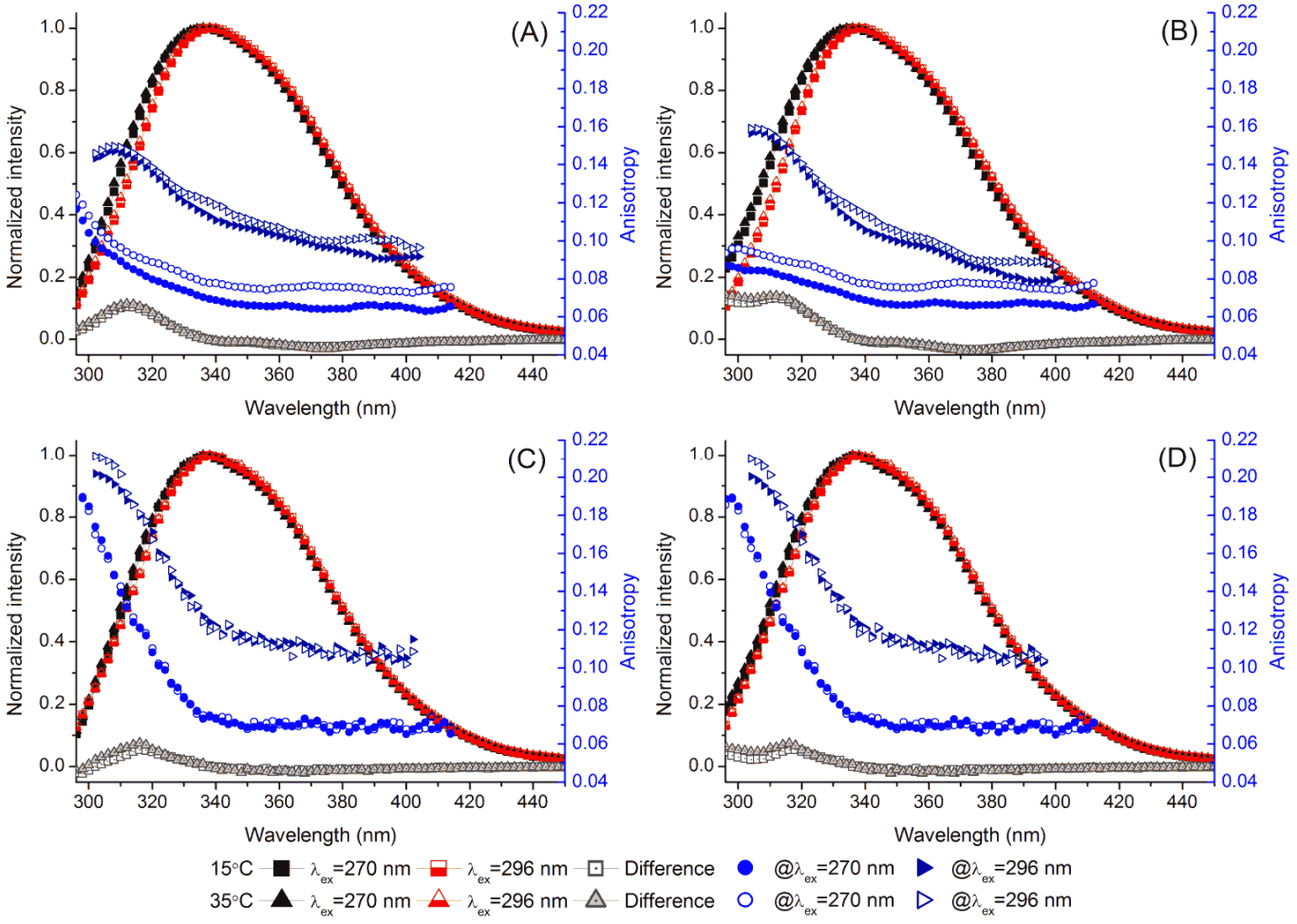

Figure 2: Normalized (Top) t-EEM$_T$ and (Bottom) EEM$_T$ emission spectra of rIgG excited at λ_{ex} 270 and 296 nm and the difference spectra (=λ_{ex} 270 − λ_{ex} 296) of the rIgG native state at two different temperatures (15° and 35°C), overlaid with the emission anisotropy at λ_{ex} 270 and 296 nm (blue circles and right pointing triangles). (A, C) Not IFE corrected. (B, D) IFE corrected using UV-Vis spectra collected at 20°C before MDF measurements.

Overall, conventional 2D spectral analysis of both t-EEM/pEEM indicated that there were very little spectral shape changes which suggest that there was no substantial structural change, and thus little change in Tyr-to-Trp FRET as expected. This was to be expected as IgG are relatively stable proteins and the detailed pEEM study has verified this [29]. Nevertheless, there were some small, yet significant differences, with a relative standard deviation (RSD) of <5.4 (t-EEM) and <5.0% (pEEM), at the blue edge (but not at the red edge) when the protein was excited at 270 and 296 nm. However, IFE correction, created an artifact that can be seen at λ_{em}<310 nm in the t-EEM and pEEM difference spectra (Figure 2, and Figure S6, SI), which may have an impact on PARAFAC modelling. This means that there is still some ambiguity with any measured data in this region.

The use of single excitation wavelengths, however, does not give the full picture and one needs to look at the full emission space, using chemometric methods to try and resolve fluorophore contributions. The first stage is to investigate how well the TSFS measurements have been at removing any scattered light contamination compared to the conventional EEM based approach. The most sensitive way of doing this

prior to PARAFAC analysis is to first look at the anisotropy maps with particular focus on the blue edge of the emission space.

3.2 *Aniso*-MDF maps of rIgG

The anisotropy variation across the rIgG emission space represented in the *aniso*-MDF maps was caused by a variety of factors such as: type and number of fluorophores present in the protein, fluorophore location in the protein, local fluorophore motion, changes in FRET, and variations in the physicochemical environment [9]. The presence of contamination from Rayleigh scattered light will also be evident as regions of abnormally high anisotropy at the blue edge of the emission. This is clearly shown in Figure 3 where the *aniso*-EEM map is much more heavily distorted as evidenced by the much higher anisotropy at the emission blue edge which also means that the weak Tyr signal is masked (Figure 4H). The differences between the *aniso*-t-EEM maps that were generated from data which was interpolated (Figure 3A), used the missing data approach, or filled with zeros (Figure 3B/C), were mainly due to reconstruction of part of the tyrosine emission region in the interpolated method (Figure 3A, black box).

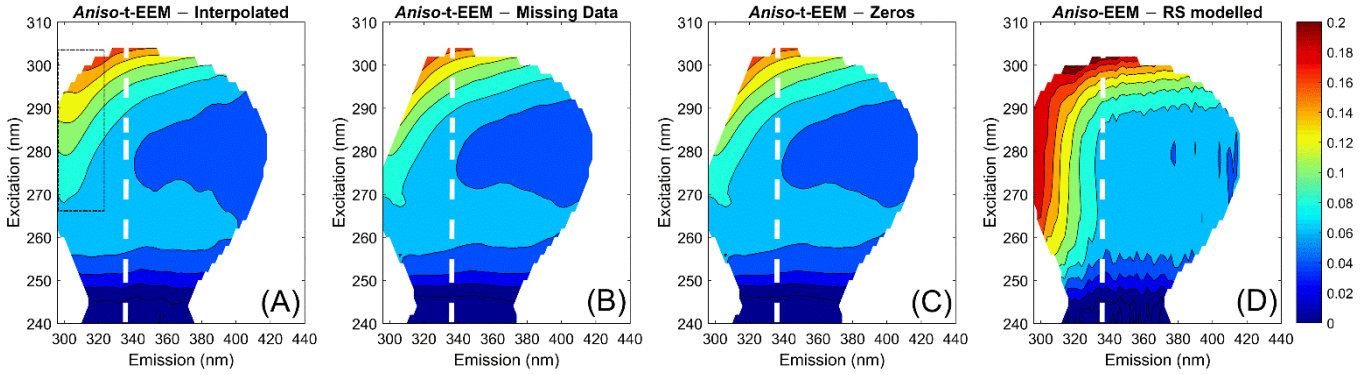

Figure 3: (A/B/C) *Aniso*-t-EEM and (D) *aniso*-EEM maps (corrected for Rayleigh scatter) of rIgG at 20°C. The white dashed lines mark the λ_{em} @336 nm excitation lines. The black box shows the Tyr region reconstructed by interpolation. The colour bar on the right represents the anisotropy scale.

When we examine the change in the *aniso*-t-EEM maps over the temperature range (Figure 4A-F), there was no significant differences (ANOVA, $p>0.05$) between the *aniso*-EEM and *aniso*-t-EEM maps in the Trp emission region, $\lambda_{em}>336$ nm, (Figure 4I). Similar to our previous study, overall there were only small changes in anisotropy at these longer wavelengths [29]. However, when we look at the changes in the mean anisotropy (Figure 4G) we see large differences (<38% difference) between the *aniso*-EEM and *aniso*-t-EEM maps which is due to residual scatter in the pEEM data. This is clear from Figure 4H-I where the differences are much greater in the Tyr emission region.

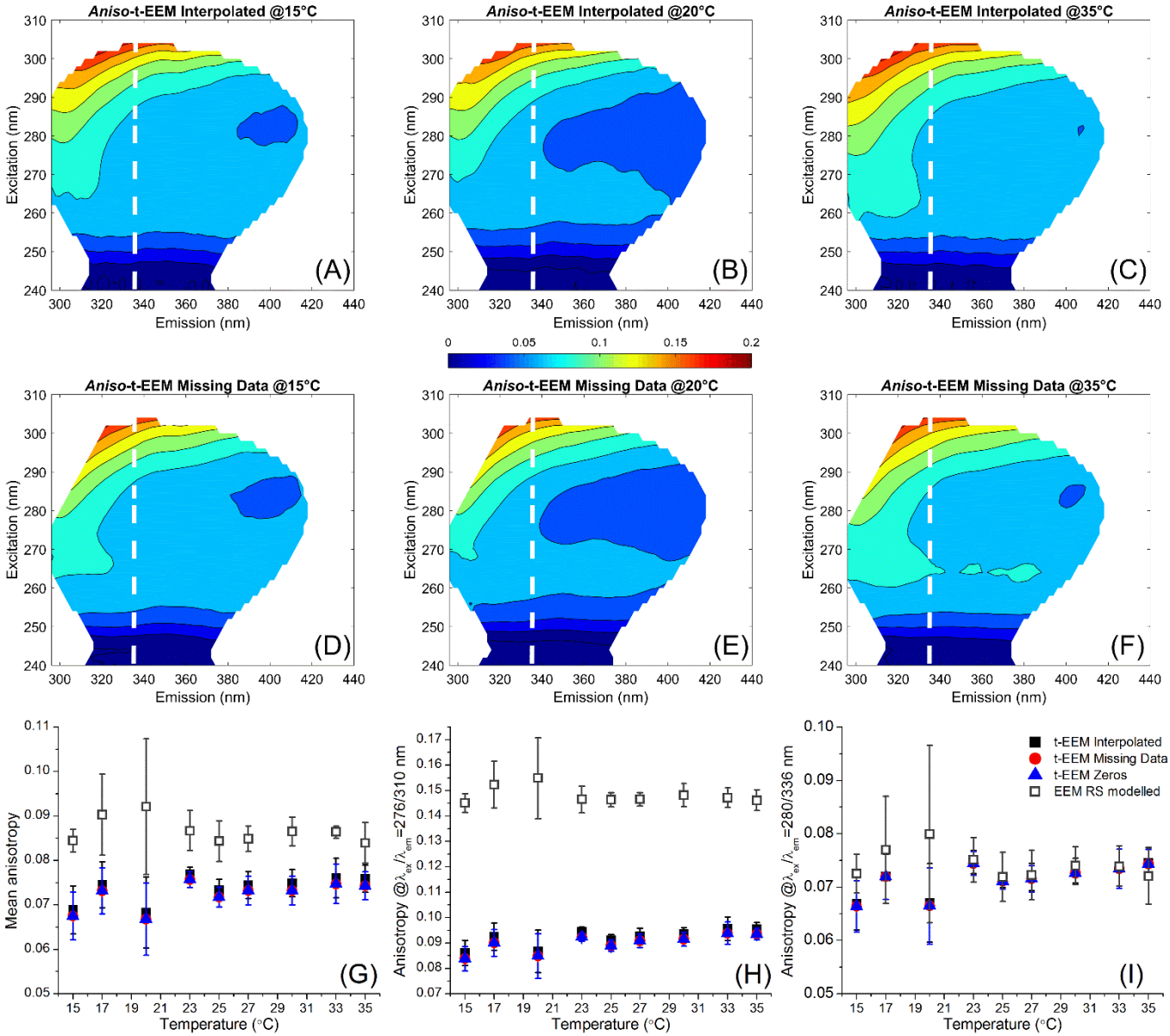

Figure 4: *Aniso*-t-EEM maps for rIgG collected at (A/D) 15°C, (B/E) 20°C, and (C/F) 35°C. *Aniso*-t-EEM maps for (top) interpolated datasets and (bottom) with missing data (<8% of data points). The white dashed lines mark the λ_{em} @336 nm. The colour bar on the middle represents the anisotropy scale. (G) Mean anisotropy ± Std Dev, (H) Tyr anisotropy at $\lambda_{ex}/\lambda_{em}$=276/310 nm ± Std Dev, and (I) Trp anisotropy at $\lambda_{ex}/\lambda_{em}$=280/336 nm ± Std Dev for the triplicate t-EEM and EEM measurements of rIgG native state.

To better assess the overall degree of change in *aniso*-MDF maps a similarity index (SimI) analysis [43] was undertaken [29], (Figure 5). Maps with SimI values >0.9 could be considered to have no significant differences from the reference spectrum, and from the 15°C measurement it was clear that the inter-replicate variation was the most significant difference observed. This was due to a combination of concentration differences (up to ~30%) coupled with varying Rayleigh scatter (amplified by the IFE correction process). This residual scattered light is present in the TSFS‖ measurements (*vide infra*). Another contributor to this variation was the fact that the experiments used multiple vials of a polyclonal rIgG and one freeze-thaw cycle [44]. SimI analysis over the full emission space clearly showed that

aniso-t-EEM maps (RSD=7.7 and 10.2% of the interpolated and missing data/zeros datasets, respectively) were more reproducible than *aniso*-EEM maps (RSD=21.50%). The improved reproducibility of the interpolated *aniso*-t-EEM data compared to the missing data or added zeros data was due to the reconstructed ASDR. For the two specific emission regions (Figure 5B/C) this variation was noticeably reduced, for the *aniso*-EEM (RSD=7.6 and 8.6% for the Tyr and Trp regions, respectively, [29]) and *aniso*-t-EEM maps (RSD~5.9 and 6.6% for the Tyr and Trp regions, respectively). This suggests that more of the temperature induced emission changes were concerned with Trp emission.

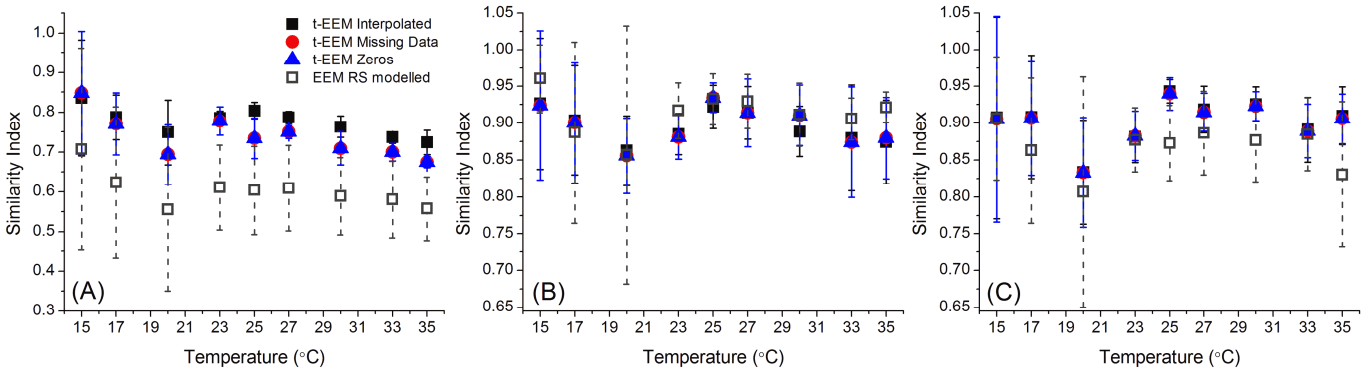

Figure 5: Plots of SimI values calculated for the various *aniso*-MDF maps over the 15−35°C temperature range. In each case, the reference spectrum was the MDF collected at 15°C from the first replicate sample (R1). (A) the full emission space; (B) the Tyr emission region ($\lambda_{ex}/\lambda_{em}$=270−290/300−320 nm); and (C) the Trp emission region ($\lambda_{ex}/\lambda_{em}$=280−300/320−360 nm). Error bars were generated from the standard deviation from triplicate measurements of the independent samples.

Also, it is important to note that the same temperature effect (small dip in SimI at 20°C, followed by an increase between 23°C and 35°C, Figures 4/5) was observed for both pEEM [29] and t-EEM data. This indicated that this effect was real because the pTSFS and pEEM datasets were collected three weeks apart (three days of measurement each), with the samples having been stored at −70°C for 11 and 14 weeks respectively. Each set of measurements used the same stock solution prepared from different vials of rIgG but with the same lot number. Changes in anisotropy were greater at lower temperatures (≤20°C), with a significant difference between replicate measurements (Figure 5). The same behavior was observed for both MDF measurements, increasing our suspicions that this was caused by a change in hydrodynamic behavior of rIgG at lower temperatures, differences in local motion, and/or flexibility of the protein structure, but we still need more evidence to support this [45, 46].

The spectral and *aniso*-map assessments above, clearly showed that changes in emission arising from structural changes/fluctuations were very small over this temperature range. It was also clear that the t-EEM measurements were much superior to pEEM because of the reduced scattered light contamination at the short emission wavelengths (<320 nm).

3.3 PARAFAC modeling of t-EEM

Meaningful PARAFAC deconvolution of intrinsic fluorophore emission from proteins is inherently challenging because of several factors: the non-linearity associated with Tyr-to-Trp FRET, emission and Rayleigh scatter overlap, particularly at short wavelengths, large differences in relative emission contributions between fluorophores, and the large numbers of fluorophores involved which only show

small spectral variation. For pEEM measurements, the scatter issue was most critical and limited the effective application of PARAFAC to resolve the Tyr emission contribution [29]. Here, the better quality of the t-EEM data at short emission wavelengths has resulted in a stronger Tyr signal (Figure 4H), which should facilitate the recovery of more than one component by PARAFAC. However, the combination of TSFS and PARAFAC analysis is not widely used [17, 30, 31] and requires first that the data is converted into an EEM like layout (t-EEM). The issue with this is to determine what is the impact of the different methods for dealing with the ASDR (i.e. the blue edge of the emission) on PARAFAC modelling.

Table 1: Comparison of the model parameters and components obtained for the normalized polarized t-EEM$_{\parallel}$, t-EEM$_{\perp}$, and unpolarized t-EEM$_T$ PARAFAC models (50 repetitions) of the rIgG native state. The spectral data were corrected using interpolation, missing data (7.9%), or filling with zeros. Samples were measured over the 15−35°C temperature range (9 temperatures × triplicate measurements).

	Interpolated			**Missing Data**			**Zeros**		
	t-EEM$_{\parallel}$	**t-EEM$_{\perp}$**	**t-EEM$_T$**	**t-EEM$_{\parallel}$**	**t-EEM$_{\perp}$**	**t-EEM$_T$**	**t-EEM$_{\parallel}$**	**t-EEM$_{\perp}$**	**t-EEM$_T$**
C1 $\lambda_{ex}/\lambda_{em}$ (nm)	280/338	280/342	280/340	280/338	280/340	280/340	280/336	280/340	280/338
C1 Fit model (%)	96.99	92.60	95.03	96.55	95.17	96.46	96.35	96.07	96.23
C2 $\lambda_{ex}/\lambda_{em}$ (nm)	278/298 (278/310[a])	278/314	278/312	320/300 (278/300[a])	276/312	278/300 (278/310[a])	276/306	276/306	276/306
C2 Fit model (%)	3.01	7.40	4.97	3.45	4.83	3.54	3.65	3.93	3.77
Variance explained ± std (%)	99.99 ($\pm 4\times10^{-9}$)	99.99 ($\pm 3\times10^{-8}$)	99.99 ($\pm 1\times10^{-8}$)	99.99 ($\pm 2\times10^{-5}$)	99.99 ($\pm 3\times10^{-9}$)	99.99 ($\pm 2\times10^{-9}$)	99.58 ($\pm 1\times10^{-5}$)	99.70[b] ($\pm 9\times10^{-8}$)	99.66 ($\pm 8\times10^{-8}$)
CONCORDIA ± std (%)	29.25 (±0.12)	31.09 (±0.52)	23.87 (±0.38)	99.80 (±0.04)	63.27 (±0.004)	65.98 (±0.003)	85.80 (±0.46)	76.53 (±0.002)	78.59 (±0.004)
Split-half analysis (%)	99.97	99.96	99.95	99.80	99.03	99.61	56.84	99.72	85.67
Iterations	7 (±16)	22 (±32)	9 (±19)	3424 (±1871)	1242 (±1)	2119 (±2)	4 (±3)	4 (±0)	4 (±0)
Time (s)	7 (±1)	10 (±1)	8 (±1)	47 (±21)	22 (±2)	30 (±2)	5 (±1)	7 (±1)	6 (±1)

[a] PARAFAC components without artifacts. [b] CONCORDIA values of local minima models were removed. One local minima model was found.

Results from PARAFAC analysis of t-EEM data were compared (Table 1, Figure 6) taking care that all the modelling was implemented under equivalent conditions. Table 1 shows that in all cases only two components were recovered (as suggested by CONCORDIA *and* split-half analysis) and that these were very similar. It was clear that all models resolved the same two fluorophores species, one associated with Trp emission (PFC1, >92−97%%) and a second weaker one (PFC2, >3−7%) which is mainly associated with Tyr emission. Analysis of the scores (Figure 7) for the un- and normalized data clearly shows that emission was quenched and that this was mainly involving the Trp emission. The increased thermally induced quenching of Trp, changed the ratio of the Tyr to Trp contributions facilitating the resolution of the two components. This was not possible with the pEEM data because of the light scatter contamination issue therefore justifying the use of pTSFS measurements.

However, there were significant differences in the profiles of the recovered fluorophore species, in particular with the weaker mostly Tyr emitting component (Figure 6, and Figure S7, SI), and this is an issue for the photophysical interpretation of the PARAFAC analysis. The differences were related to the ASDR pre-processing methods and their effect on the short Stokes shifted emission region. PFC1 (Trp) was virtually identical in terms of the recovered spectral profiles, except for the models filled with zeros. The insertion of zeros method restricted PARAFAC to an abnormal solution which led to an underestimation of the blue edge emission of the Trp fluorophores [42]. This method facilitated PARAFAC convergence (lowest number of iterations, Table 1), but it could cause premature deconvolution, increasing the variability of the spectral profiles of the calculated models. Thus, insertion of zeros slightly underestimated both Trp and Tyr relative contributions (Figure 6H/I) compared to the other methods.

When the missing data approach to ASDR was implemented, PARAFAC was free to better estimate the continuous shape of Trp and Tyr emission. This was because it did not restrict or modify the data, and thus better extracted spectral profiles which might be a truer representation of the actual emission. The missing data method did, however, create some artifacts at the emission blue edge (Figure 6F) which was amplified by the IFE correction as shown in the excitation slab corresponding to PFC2 emission and this was particularly severe for the parallel polarized light data (Figure S7B, SI). The use of interpolation significantly decreased the required computational time and led to a resolution that appears to be spectrally acceptable. However, CONCORDIA values were reduced for the interpolated data compared to the other methods, which was caused by extension of emission into the ASDR and thus increased emission overlap (Figure 6, and Figure S9, SI). One might expect that this suggests that three components should be recoverable by PARAFAC (Tyr, Trp from hydrophobic locations, and Trp externally located on the protein). However, the three component PARAFAC models (Table S1, SI) did not show any improvement in the model performance quality parameters.

Differences in quality and model parameters between the different polarizations (Table 1, and Figure S7, SI) for the missing and interpolated t-EEM methods were related to sample spectral characteristics, and specifically the intrinsic anisotropy of the emission from the large protein molecule, and the degree of FRET. This is clear to see when ~~the~~ one compares the $TSFS_T$ results with the pTSFS models in the table above. The parallel polarization measurements are more directly sensitive to Tyr-Trp FRET (i.e. lower PFC2 scores) and to the presence of residual scatter. This is due to a combination of factors including the short fluorescence lifetime of tyrosine (<4 ns) coupled with the long, 26 ns, rotational correlation time of rIgG [47]. In the t-EEM$_{\parallel}$ models, it was clear that there was an element of the spectral profile that could be assigned to Rayleigh light scatter which was amplified by the IFE correction (PFC2 blue shifted). In the t-EEM$_{\perp}$ models there was a clear shoulder at ~350 nm (Figure 6, and Figure S7, SI) due to Trp emission which resulted in a higher score (~5−7%) for this component (Table 1, Figure S8, SI). PFC2 scores for the t-EEM$_{\perp}$ were higher for the interpolated (~7%) than the missing data (~5%), suggesting that the interpolation method improved the resolution of Tyr emission. In contrast, there were no significant differences between the polarized and unpolarized t-EEM PARAFAC using the data filled with zeros, which is surprising, as there are real differences between the polarized and unpolarized spectra of rIgG. This therefore rules out the use of this ASDR correction procedure for intrinsic protein fluorescence analysis.

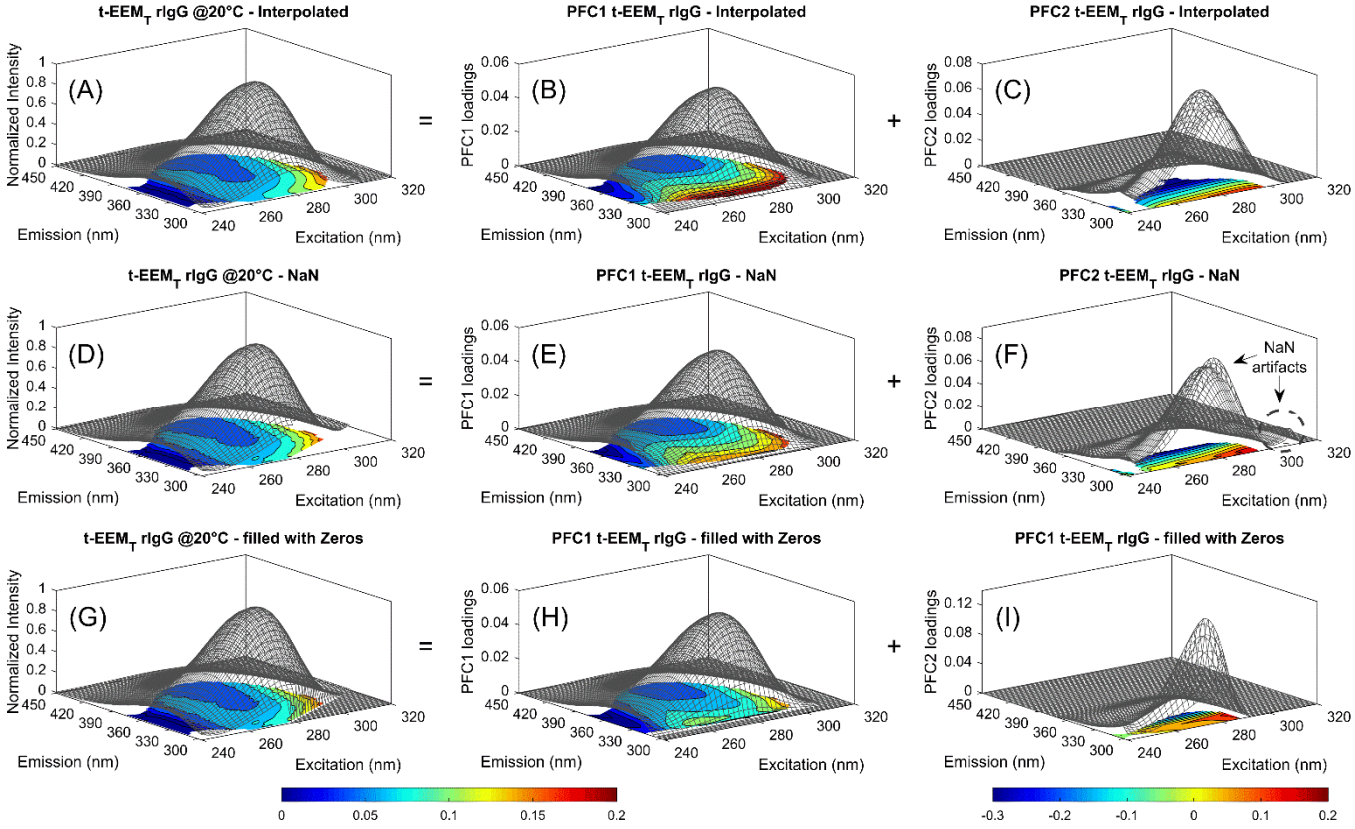

Figure 6: Comparison of PARAFAC modelling of the t-EEM$_T$ rIgG native structure data (A) interpolated, (D) missing data (NaN), and (G) filled with zeros. PFC1 (Trp) was virtually identical for the datasets with (B) interpolation, (E) missing data and (H) filled with zeros. Even if PFC2 resolved the Tyr signal for the (D) interpolated, (F) missing data and (I) filled with zeros, there were slight differences caused by the presence of missing data and zeros. t-EEM$_T$ landscapes overlapped with *aniso*-t-EEM maps for rIgG measured at 20°C. The colour bars on the bottom represent the anisotropy scale.

For better analysis of protein structural change, it would be useful to be able to fully resolve the Trp and Tyr emission [9, 12, 14], to provide both spectral profiles and relative contribution values. Analysis of the PARAFAC components, PFC1 (Trp) and PFC2 (Tyr) scores from the un-normalized t-EEM$_T$ data from each method showed a linear decrease with increasing temperature due to quenching (Figure 7A/B). The trends were the same for all three data handling methods with no significant differences (ANOVA, $p>0.05$) in PFC1/2 scores trends, indicating that any of the PARAFAC scores could be used to monitor structural/concentration changes (r Pearson>0.99). The error bars in Figure 7A/B were due to differences in protein concentration between the replicate samples (~31%), which is why the normalized data is better for investigating structural changes.

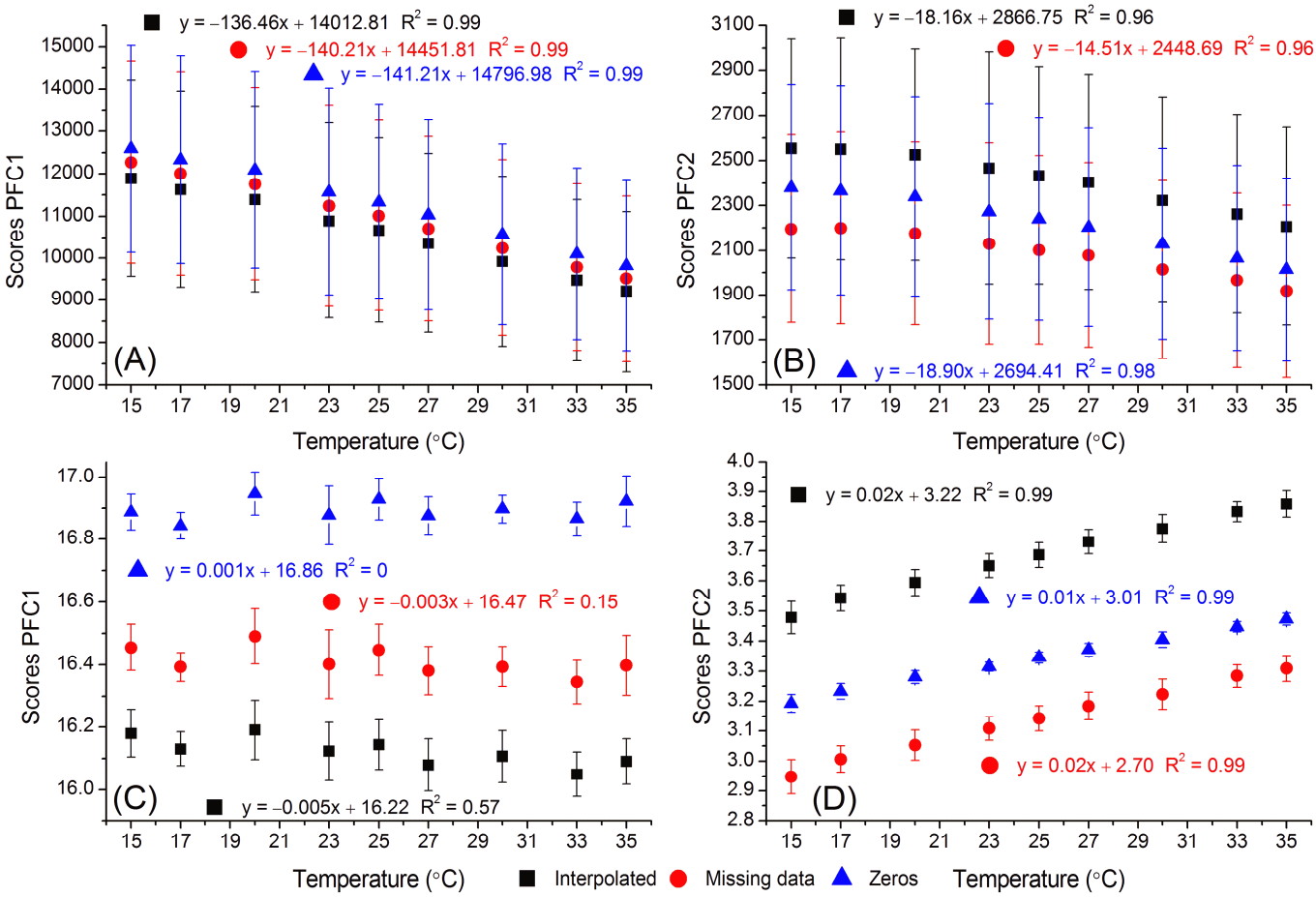

Figure 7: Scores plots of two-component PARAFAC models for the: (top) non-normalized, and (bottom) normalized unpolarized rIgG t-EEM$_T$ datasets with the different ASDR treatment methods.

Normalization removed variations caused by small protein concentration differences and instrument measurement error, and this was reflected in the smaller error bars (~1%) obtained for PARAFAC scores (Figure 7C/D). Although the Trp (PFC1) trends showed that there were no significant structural changes in the rIgG over the 15° to 35°C temperature range, while the PFC2 scores (Tyr emission) increased very slightly with increasing temperature (Figure 7D) due to Trp quenching. The only significant differences in the scores for the different ASDR methods was that the interpolated data generally had higher PFC2 scores. This would suggest that this was the best option for producing protein fluorescence data suitable for PARAFAC modelling to monitor subtle changes in protein behavior and structure via changes in the ratio between Tyr and Trp emission. Here, the structural changes are very small, and the increased thermal motion generates a linear decrease in emission intensity due to quenching of Trp emission.

4 Conclusions

We have demonstrated that pTSFS is a better measurement method than pEEM for PARAFAC analysis of intrinsic protein fluorescence, and in particular at the blue edge of the emission related to Tyr fluorescence. This is because TSFS minimized the collection of Rayleigh scattered light which caused a lot of problems at the emission blue edge in EEM spectra, largely due to the difficulty in removing the

Rayleigh shot noise [29]. A simple transformation of pTSFS data into an pEEM like layout (t-EEM) provided the trilinear structure [30] required for PARAFAC analysis. However, the t-EEM transformation, produced an ASDR (<8%) at the blue edge of the emission which is critical for resolving Tyr emission. Evaluation of several data handling methods, missing data, use of zeros, and interpolation, to deal with this issue revealed that PARAFAC results were very method dependent. From a spectroscopic perspective, in each case PARAFAC separated Tyr from Trp emission, thus, confirming the superior performance of TSFS measurements compared to EEM [29].

This study showed that significantly different PARAFAC outputs (spectral profiles and scores) were obtained when using different methods for dealing with ASDR. The use of zeros and missing data to fill the ASDR both produced PARAFAC models which potentially underestimated the relative contribution of the Tyr component (Figure 7). Both methods were susceptible to producing spectral artifacts, particularly at the blue edge of the emission where the noise and light scatter contamination was an issue. One drawback for the use of missing data was the high computational time required for this method, making it prohibitive for online or inline applications. The most suitable option, t-EEM in combination with interpolation generated the best quality PARAFAC models from the point of view of the spectral profiles and scores recovered. However, one must be cautious when interpreting this data and in particular the spectral profiles as the validation of PARAFAC output from intrinsic protein emission is still unproven (although known for small molecule examples). What has been proven here is that the general spectral trends observed in the scores were similar but the magnitudes significantly different and thus when using scores plots to follow protein changes one might be advised to use a combination of two ASDR approaches (missing data and interpolation) to ensure a useable model outcome for analytical purposes (*e.g.* protein stability studies, IgG product variance, etc.).

The PARAFAC modelling also suggested that there was still some residual scattered light in the pTSFS data (which is unsurprising given the 10 nm slit widths used). This was seen in the different profiles recovered for the second component (mostly Tyr) in the $TSFS_{\parallel}$ and $TSFS_{\perp}$ data. Ultimately, this indicated that to extract a true uncontaminated Tyr emission component, and thus accurate scores, one needs to use narrower slits, which will decrease signal intensity which can only be recovered by increasing acquisition time, which is not practical currently for ARMES using conventional benchtop spectrometers where four measurements are required (and particularly for rapid or high throughput analytical applications). The $TSFS_{\perp}$ measurement offered the best quality data for modelling Tyr/Trp emission because it had the least amount of residual scattered light and thus generated the most reasonable estimate of the true contributions of each fluorophore to the total emission. However, the second $TSFS_{\perp}$ recovered component still does not represent Tyr only emission and there is some associated Trp emission present. Despite this, the ratio of PARAFAC scores generated by these pTSFS/PARFAC models provides a unique and robust tool for assessing the change in emission caused by structural changes impacting on FRET.

In conclusion, this study, when considered with our previous EEM study [29], has shown that the combination of pTSFS measurements, with precisely defined pre-processing, and PARAFAC modelling is the most suitable method for the analysis of intrinsic protein fluorescence. The pTSFS based methodology shows sufficient sensitivity to extract signals from Tyr emission which is key to being able to observe and measure subtle changes in protein structure [8]. This is of particular importance for

understanding the mechanisms of aggregation [48] and protein degradation which are fundamental to the delivery of safe biotherapeutic agents.

5 Supplemental information available

Supporting information is available which provides additional spectral data further details on the chemometric analysis. This is available online at: https://ars.els-cdn.com/content/image/1-s2.0-S0169743919304630-mmc1.docx

6 Acknowledgements

This publication has emanated from research supported in part by a research grant from Science Foundation Ireland (SFI) and is co-funded under the European Regional Development Fund under Grand number (14/IA/2282, *Advanced Analytics for Biological Therapeutic Manufacture*, to AGR). We also thank Agilent Technologies (Mulgrave Victoria, Australia) for the loan of a fluorescence spectrometer.

7 Declarations of interest:

None to report.

8 References

[1] J.R. Lakowicz, Principles of Fluorescence Spectroscopy, 3rd Edition ed., Springer, New York, 2006.

[2] J.M. Reichert, Marketed therapeutic antibodies compendium, Mabs, 4 (2012) 413-415.

[3] D.M. Ecker, S.D. Jones, H.L. Levine, The therapeutic monoclonal antibody market, Mabs, 7 (2015) 9-14.

[4] B. Sharma, Immunogenicity of therapeutic proteins. Part 1: Impact of product handling, Biotechnol. Adv., 25 (2007) 310-317.

[5] K. Wiberg, A. Sterner-Molin, S.P. Jacobsson, Simultaneous determination of albumin and immunoglobulin G with fluorescence spectroscopy and multivariate calibration, Talanta, 62 (2004) 567-574.

[6] E.A. Burstein, N.S. Vedenkina, M.N. Ivkova, Fluorescence and Location of Tryptophan Residues in Protein Molecules, Photochem. Photobiol., 18 (1973) 263-279.

[7] P. Garidel, M. Hegyi, S. Bassarab, M. Weichel, A rapid, sensitive and economical assessment of monoclonal antibody conformational stability by intrinsic tryptophan fluorescence spectroscopy, Biotechnology Journal, 3 (2008) 1201-1211.

[8] L. Liu, L.J. Braun, W. Wang, T.W. Randolph, J.F. Carpenter, Freezing-Induced Perturbation of Tertiary Structure of a Monoclonal Antibody, J. Pharm. Sci., 103 (2014) 1979-1986.

[9] R.C. Groza, B.Y. Li, A.G. Ryder, Anisotropy resolved multidimensional emission spectroscopy (ARMES): A new tool for protein analysis, Anal. Chim. Acta, 886 (2015) 133-142.

[10] K. Ohadi, R.L. Legge, H.M. Budman, Intrinsic fluorescence-based at situ soft sensor for monitoring monoclonal antibody aggregation, Biotechnol. Progr., 31 (2015) 1423-1432.

[11] G. Weber, Fluorescence-polarization spectrum and electronic-energy transfer in tyrosine, tryptophan and related compounds, Biochem. J, 75 (1960) 335-345.

[12] J. Eisinger, Intramolecular Energy Transfer in Adrenocorticotropin, Biochemistry, 8 (1969) 3902-&.

[13] H.C. Chiu, R. Bersohn, Electronic-Energy Transfer Between Tyrosine and Tryptophan in Peptides Trp-(Pro)N-Tyr, Biopolymers, 16 (1977) 277-288.

[14] S. Bobone, M. van de Weert, L. Stella, A reassessment of synchronous fluorescence in the separation of Trp and Tyr contributions in protein emission and in the determination of conformational changes, J. Mol. Struct., 1077 (2014) 68-76.

[15] I.M. Warner, G.D. Christian, E.R. Davidson, J.B. Callis, Analysis of Multicomponent Fluorescence Data, Anal. Chem., 49 (1977) 564-573.

[16] D. Patra, A.K. Mishra, Recent developments in multi-component synchronous fluorescence scan analysis, Trac-Trends in Analytical Chemistry, 21 (2002) 787-798.

[17] K. Kumar, A.K. Mishra, Analysis of dilute aqueous multifluorophoric mixtures using excitation-emission matrix fluorescence (EEMF) and total synchronous fluorescence (TSF) spectroscopy: A comparative evaluation, Talanta, 117 (2013) 209-220.

[18] B. Li, P.W. Ryan, M. Shanahan, K.J. Leister, A.G. Ryder, Fluorescence excitation-emission matrix (EEM) spectroscopy for rapid identification and quality evaluation of cell culture media components, Appl. Spectrosc., 65 (2011) 1240-1249.

[19] B. Li, M. Shanahan, A. Calvet, K.J. Leister, A.G. Ryder, Comprehensive, quantitative bioprocess productivity monitoring using fluorescence EEM spectroscopy and chemometrics, Analyst, 139 (2014) 1661-1671.

[20] Y. Casamayou-Boucau, A.G. Ryder, Extended wavelength anisotropy resolved multidimensional emission spectroscopy (ARMES) measurements: better filters, validation standards, and Rayleigh scatter removal methods, Methods Appl Fluoresc, 5 (2017) 037001.

[21] H. Abdollahi, R. Tauler, Uniqueness and rotation ambiguities in Multivariate Curve Resolution methods, Chemometrics Intellig. Lab. Syst., 108 (2011) 100-111.

[22] C. Ruckebusch, L. Blanchet, Multivariate curve resolution: A review of advanced and tailored applications and challenges, Anal. Chim. Acta, 765 (2013) 28-36.

[23] R. Bro, PARAFAC. Tutorial and applications, Chemometrics Intellig. Lab. Syst., 38 (1997) 149-171.

[24] C.M. Andersen, R. Bro, Practical aspects of PARAFAC modeling of fluorescence excitation-emission data, J. Chemom., 17 (2003) 200-215.

[25] K.R. Murphy, C.A. Stedmon, D. Graeber, R. Bro, Fluorescence spectroscopy and multi-way techniques. PARAFAC, Analytical Methods, 5 (2013) 6557-6566.

[26] S.D. Brown, L.A. Sarabia, J. Trygg, Comprehensive chemometrics chemical and biochemical data analysis, Amsterdam : Elsevier, Amsterdam, 2009.

[27] J.M. Amigo, F. Marini, Multiway Methods, in: F. Marini (Ed.) Chemometrics in Food Chemistry, Elsevier Science Bv, Amsterdam, 2013, pp. 265-313.

[28] R.C. Groza, A. Calvet, A.G. Ryder, A fluorescence anisotropy method for measuring protein concentration in complex cell culture media, Analytica Chimica Acta, 821 (2014) 54-61.

[29] M. Steiner-Browne, S. Elcoroaristizabal, Y. Casamayou-Boucau, A.G. Ryder, Investigating native state fluorescence emission of Immunoglobulin G using polarized Excitation Emission Matrix (pEEM) spectroscopy and PARAFAC, Chemometrics and Intelligent Laboratory Systems, 185 (2019) 1-11.

[30] K. Kumar, A.K. Mishra, Application of parallel factor analysis to total synchronous fluorescence spectrum of dilute multifluorophoric solutions: Addressing the issue of lack of trilinearity in total synchronous fluorescence data set, Anal. Chim. Acta, 755 (2012) 37-45.

[31] K. Kumar, A.K. Mishra, Parallel factor (PARAFAC) analysis on total synchronous fluorescence spectroscopy (TSFS) data sets in excitation-emission matrix fluorescence (EEMF) layout: Certain practical aspects, Chemometrics Intellig. Lab. Syst., 147 (2015) 121-130.

[32] S. Elcoroaristizabal, R. Bro, J.A. Garcia, L. Alonso, PARAFAC models of fluorescence data with scattering: A comparative study, Chemometrics Intellig. Lab. Syst., 142 (2015) 124-130.

[33] K. Kumar, A.K. Mishra, Multivariate curve resolution alternating least square (MCR-ALS) analysis on total synchronous fluorescence spectroscopy (TSFS) data sets: Comparing certain ways of arranging TSFS-based three-way array, Chemometrics Intellig. Lab. Syst., 147 (2015) 66-74.

[34] Y. Casamayou-Boucau, A.G. Ryder, Accurate anisotropy recovery from fluorophore mixtures using Multivariate Curve Resolution (MCR), Anal. Chim. Acta, 1000 (2018) 132-143.

[35] K. Kumar, A.K. Mishra, Understanding the effect of calibration set design for the application of MCR-ALS analysis on excitation-emission matrix fluorescence (EEMF) data sets under commonly used non-negativity constraints, Chemometrics and Intelligent Laboratory Systems, 149 (2015) 70-77.

[36] S. Elcoroaristizabal, A. de Juan, J.A. Garcia, N. Durana, L. Alonso, Comparison of second-order multivariate methods for screening and determination of PAHs by total fluorescence spectroscopy, Chemometrics and Intelligent Laboratory Systems, 132 (2014) 63-74.

[37] M.R. Eftink, L.A. Selvidge, P.R. Callis, A.A. Rehms, Photophysics of indole-derivatives - experimental resolution of La and Lb transition and comparison with theory, J. Phys. Chem., 94 (1990) 3469-3479.

[38] M. Ameloot, M. vandeVen, A.U. Acuna, B. Valeur, Fluorescence anisotropy measurements in solution: Methods and reference materials (IUPAC Technical Report), Pure Appl. Chem., 85 (2013) 589-608.

[39] D.N. Kothawala, K.R. Murphy, C.A. Stedmon, G.A. Weyhenmeyer, L.J. Tranvik, Inner filter correction of dissolved organic matter fluorescence, Limnology And Oceanography-Methods, 11 (2013) 616-630.

[40] M. Tarai, A.K. Mishra, Inner filter effect and the onset of concentration dependent red shift of synchronous fluorescence spectra, Anal. Chim. Acta, 940 (2016) 113-119.

[41] G. Tomasi, R. Bro, PARAFAC and missing values, Chemometrics and Intelligent Laboratory Systems, 75 (2005) 163-180.

[42] L.G. Thygesen, A. Rinnan, S. Barsberg, J.K.S. Moller, Stabilizing the PARAFAC decomposition of fluorescence spectra by insertion of zeros outside the data area, Chemometrics Intellig. Lab. Syst., 71 (2004) 97-106.

[43] B. Li, A.G. Ryder, Similarity Index: a Rapid Classification Method for Multivariate Data Arrays, US7983874B2, 2011.

[44] D.C. Hanson, J. Yguerabide, V.N. Schumaker, Segmental flexibility of immunoglobulin-G antibody molecules in solution - a new interpretation, Biochemistry, 20 (1981) 6842-6852.

[45] K. Lim, D.M. Jameson, C.A. Gentry, J.N. Herron, Molecular-dynamics of the antifluorescein-4-4-20 antigen-binding fragment. 2. Time-resolved fluorescence spectroscopy, Biochemistry, 34 (1995) 6975-6984.

[46] T.J. Kamerzell, J.D. Ramsey, C.R. Middaugh, Immunoglobulin dynamics, conformational fluctuations, and nonlinear elasticity and their effects on stability, Journal of Physical Chemistry B, 112 (2008) 3240-3250.

[47] V.P. Timofeev, I.V. Dudich, Y.K. Sykulev, R.S. Nezlin, Rotational Correlation Times of IgG and its Fragments Spin-Labeled at Carbohydrate or Protein Moieties - Spatially Fixed Position of Fc Carbohydrate, FEBS Lett., 89 (1978) 191-195.

[48] Z. Hamrang, N.J.W. Rattray, A. Pluen, Proteins behaving badly: emerging technologies in profiling biopharmaceutical aggregation, Trends Biotechnol., 31 (2013) 448-458.